Journal of Magnetics 10(4), 157-162 (2005)

Irreversible Magnetization of MgB_2 Superconductor

Mun-Seog Kim*, Kyu-Tae Kim, Wan-Seop Kim, Po Gyu Park, Kyu Won Lee, and Sung-Ik Lee[1]

Division of Electromagnetic Metrology, Korea Research Institute of Standards and Science, P. O. BOX 102, Yuseong, Daejeon 305-600, Korea

[1]Department of Physics, Pohang University of Science and Technology, Pohang 790-784, Korea

(Received November 28, 2005)

We report the magnetic-field dependence of the irreversible magnetization of binary superconductor MgB_2. For the temperature region of $T < 0.9T_c$, the contribution of the bulk pinning to the magnetization overwhelms that of the surface pinning. This was evident from the fact that the magnetization curves, $M(H)$, were well described by the critical-state model without considering the reversible magnetization and the surface pinning effect. It was also found that the $M(H)$ curves at various temperatures scaled when the field and the magnetization were normalized by the characteristic scaling factors $H^*(T)$ and $M^*(T)$, respectively. This feature suggests that the pinning mechanism determining the hysteresis in $M(H)$ is unique below $T = T_c$.

Key words : MgB_2, irreversible magnetization, the exponential critical-state model, flux jumping, irreversibility line, surface barrier

1. Introduction

In the mixed state, the magnetization of superconductors is a combination of two different contributions, M_{eq} and M_{irr}. M_{eq} is the equilibrium or reversible magnetization [1] and M_{irr} is the irreversible magnetization. The former is caused by the equilibrium surface current. The latter arises from the surface (Bean-Livingston) barrier effect [2], as well as the bulk pinning due to the interaction between vortices andvarious defects within the superconductor. The surface barrier originates from the competition between two forces, an attractive interaction between a vortex and its image vortex and a repulsive interaction between a vortex and the surface-shielding current. For high-T_c cuprate superconductors, the irreversible magnetization at low temperatures is dominated by the bulk pinning. However, the role of the surface-barrier effect becomes significant as the temperature approaches toward T_c [3].

In this work, we measured the magnetization $M(H)$ of MgB_2 superconductor [4] as a function of the external magnetic field to elucidate its pinning properties in detail. A prominent flux-jumping effect at low temperatures due to a low thermal conductivity of the material [5] was observed, which was reflected by abrupt changes of magnetization when external magnetic field varies.

Except for the flux-jumping region, the $M(H)$ curves for various temperatures were successfully described by the exponential critical-state model [6]. The $M(H)$ curves up to $T/T_c = 0.9$ were scaled to a single universal curve with the characteristic scaling factors, $H^*(T)$ and $M^*(T)$, implying a significant role of bulk pinning in our experimental window. In addition, we found that the characteristic field $H^*(T)$, proportional to the irreversible line $H_{irr}(T)$ in vortex-phase diagram, was not described by the $H_{irr} \sim (1 - T/T_c)^n$ ($n \geq 1.5$) [7], which was in sharp contrast to the cuprates.

2. Experiments

Details on the sample preparation are given elsewhere [8]. A stoichiometric mixture of Mg and B (99.97%, Alfa Aesar) was ground in a glove bag filled with Ar gas. The resulting precursor was palletized, wrapped in Ta foil, and put into a high-pressure cubic cell. It was pressed up to 3.5 GPa at 950°C for 2 hours, and then quenched to room temperature. The dimensions of the sample were 2.03 mm long and 4.25 mm in diameter. The magnetization curves were measured by using a superconducting quantum inter-

*Corresponding author: Tel: +82-42-868-5725,
e-mail: msk2003@kriss.re.kr

ference device magnetometer (Quantum Design, MPMS-*XL*).

3. Results and Discussion

Figure 1 shows the temperature dependence of the magnetic susceptibility, $4\pi\chi$(T), which is measured in external field, H_{ext} = 5 Oe, parallel to principle axis of the cylindrical sample. This figure reveals that the superconducting transition occurs at 38.6 K and the transition width is less than 1 K. At low temperatures, the absolute value of $4\pi\chi$ for ZFC curve is close to 2.0, while the value for FC curve is about 0.1. This pronounced difference reflects a strong vortex pinning in this material. For s superconductor, the low-field susceptibility is written by $4\pi\chi = 4\pi M/H_{ext} = 1/(d-1)$, where the demagnetization factor, d, can vary with relative direction of the external field to the principle axis of the sample. From this formula and the low-temperature susceptibility for ZFC curve, the demagnetization factor of the sample is deduced to be $d = 0.51$. This value is quite close to 0.54 calculated from the sample dimensions, 2.03 mm long and 4.25 mm in diameter, using the Orborn formula [9]. This accordance says that the coupling between grains consisting of the sample is quite strong, and thus the demagnetization effect is governed by the outward appearance of the sample, not by the size and the shape of each grains. In other words, the sample shows a bulk superconductivity, even though the grain boundaries exist. As we mentioned in previous section, our sample was synthesized by the high-pressure technique under a high

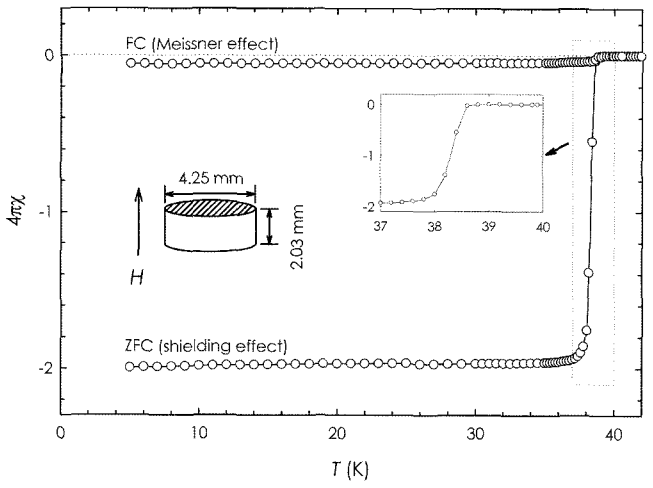

Fig. 1. Temperature dependence of the magnetic susceptibility, $4\pi\chi(T)$, measured in external field, H_{ext} = 5 Oe, parallel to principle axis of the cylindrical sample. $4\pi\chi$ data were taken in both zero-field-cooled (shielding) and field-cooled (Meissner) conditions. Inset: $4\pi\chi(T)$ (ZFC) around transition region.

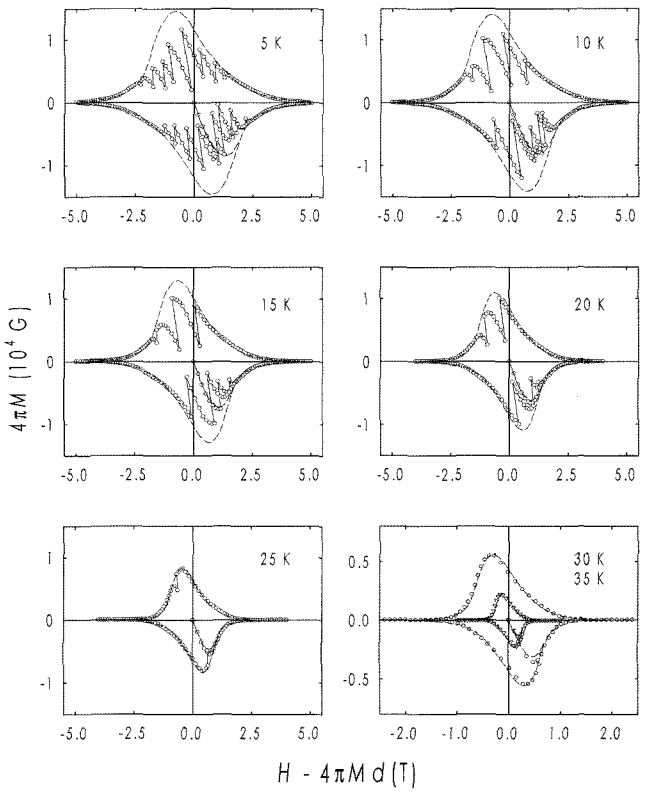

Fig. 2. Magnetization curves, $4\pi M(H)$, measured in the region of 5 K ≤ T ≤ 35 K and −5 T ≤ H ≤ 5 T. The dashed lines represent the theoretical curve for the exponential critical-state model.

temperature, which might make the strong grain coupling possible.

Figure 2 shows $4\pi M(H)$ curves measured at various temperatures. In the figure, the x-axes for H were corrected by the demagnetization factor $d = 0.51$ obtained from Fig. 2. Below 25 K, the saw-tooth behavior is clearly seen at relatively low-field region due to the flux jumps [5, 10]. In the critical state, a small perturbation of temperature could give rise to increase the sample temperature. As a result, the screening-current density is diminished, which is accomplished by redistribution of vortices inside the superconductor. This precess results in the perturbation of electric field and thereby generation of an additional heat. Since the thermal conductivity of MgB_2 is not so high [5], the additional heat release due to the flux motion is not removed effectively. Thus the critical state becomes unstable and the flux jumps occur, causing instability of magnetization.

The irreversible magnetization can be described by various critical-state models [6, 11, 12]. Bean's critical-state model [12] has been widely used to describe the magnetization and to calculate the critical-current density for superconducting materials. The model assumes that

the slope $dh(r)/dr$ is a constant and field independent, where $h(r)$ denotes the local magnetic induction inside a sample. Therefore, the critical-current density or the irreversible magnetization should also be field independent, which is contrary to the experiments. Here, we employ the exponential critical-state model [6] to describe the magnetization properly, which takes into account the field dependence of the critical-current density.

In the frame of the exponential model, the critical-current density, $J_c(h(r))$, is given by

$$J_c(h(r)) = J_0 \exp(-|h(r)|/H_0), \quad (1)$$

where J_0 and H_0 are adjustable parameters which depend on material. According to Ampere's law, the field gradient inside a sample is given by

$$\frac{dh(r)}{dr} = -\mathrm{sgn}(J)\frac{4\pi}{c}J_c(h(r)), \quad (2)$$

where $\mathrm{sgn}(x)$ is the sign function and c is the speed of light.

For an infinitely long cylindrical superconductor with radius a, we solve Eq. (2) and calculate the irreversible magnetization. In the calculation, the demagnetization effect is irrelevant, since the applied field H is parallel to principle axis of a long cylinder. To get a complete picture of the critical states, five different cases according to the external-field regime should be considered.

Case I: $0 \le H \le H_p$ in increasing-field branch

As the external magnetic field increases from 0 to H_p, the vortices can penetrate into the sample. (Here, we assume the lower critical field, H_{c1}, to be zero, which is valid when $|H_{irr}| >> |H_{eq}|$.) The penetrated vortices are distributed in the region between r_1 and a ($0 \le r_1 \le$ a), where the r_1 is zero at $H = H_p$. The solution for $h(r)$ is given by

$$h(r) = \begin{cases} 0 & \text{for } 0 \le r \le r_1 \\ H_0 \ln[(J_0 r + c_0)/H_0] & \text{for } r_1 \le r \le a \end{cases}.$$

The boundary conditions $h(a) = H$ and $h(r_1) = 0$ give the integration coefficient c_0, the field boundary r_1, and the H_p,

$$c_0 = H_0 \exp(H/H_0) - J_0 a$$
$$r_1 = (H_0 - c_0)/J_0$$
$$H_p = H_0 \ln(J_0 a/H_0 + 1).$$

Case II: $H_p \le H \le H_{max}$ in increasing-field branch

For $H \ge H_p$, the vortices are distributed in the whole region of $0 \le r \le a$. The solution for this case is the same as that in case I, if the r_1 is replaced by zero. The H_{max} denotes the maximum value of the applied field.

Case III: $H_{max} \ge H \ge H_r$ in decreasing-field branch

When the external field decreases from H_{max}, the distribution of vortices in the sample is given by

$$h(r) = \begin{cases} H_0 \ln[(J_0 r + c_{max})/H_0] & \text{for } 0 \le r \le r_2 \\ H_0 \ln[(-J_0 r + c_1)/H_0] & \text{for } r_2 \le r \le a \end{cases}.$$

While the $h(r)$ in the region of $0 \le r \le r_2$ is determined by H_{max} in the previous case, the external field determines $h(r)$ in $r_2 \le r \le a$. The signs of slope $dh(r)/dr$ in the two regions differ from each other. For $H = H_r$, the r_2 becomes zero. From the boundary condition $h(a) = H$ and the continuity condition at $r = r_2$, the parameters c_{max}, c_1, r_2, and H_r are given by

$$c_{max} = H_0 \exp(H_{max}/H_0) - J_0 a$$
$$c_1 = H_0 \exp(H/H_0) + J_0 a$$
$$r_2 = (c_1 - c_{max})/2J_0$$
$$H_r = H_0 \ln[\exp(H_{max}/H_0) - 2J_0 a/H_0].$$

Case IV: $H_r \ge H \ge 0$ in decreasing-field branch

In this case, the external field decreases from H_r to zero. Even at zero field, however, the supercurrent flows through the entire region of $0 \le r \le a$. This current determines the residual (remanent) magnetization. The solution is given by

$$h(r) = H_0 \ln[(-J_0 r + c_2)/H_0] \text{ for } 0 \le r \le a.$$

The boundary condition $h(a) = H$ gives the parameter c_2,

$$c_2 = H_0 \exp(H/H_0) + J_0 a.$$

Case V: $0\ H \ge -H_p$ in decreasing-field branch

For $r \ge r_3$, the flux distribution is described by the same manner as in the case I. However, for $r \le r_3$, the distribution is governed by the residual vortices. The solution is given by

$$h(r) = \begin{cases} H_0 \ln[(-J_0 r + c_3)/H_0] & \text{for } 0 \le r \le r_3 \\ -H_0 \ln[(J_0 r - c_4)/H_0] & \text{for } r_3 \le r \le a \end{cases}.$$

From the boundary condition $h(a) = H$ and the continuity condition at $r = r_3$, the parameters c_3, c_4, and r_3 are given by

$$c_3 = H_0 +) - J_0 r_3$$
$$c_4 = -H_0 \exp(-H/H_0) + J_0 a$$
$$r_3 = (H_0 + c_4)/J_0.$$

Other Cases

There are additional cases for a complete hysteresis

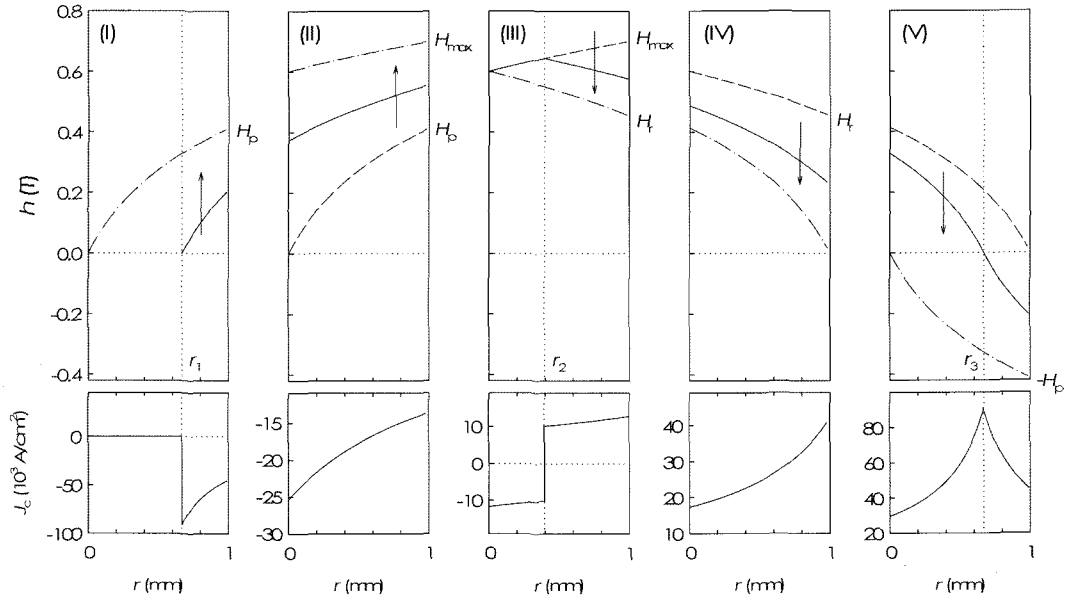

Fig. 3. Distributions of vortices, $h(r)$, and supercurrent density, $J_c(r)$, inside a cylindrical superconductor in the frame of the exponential critical-state model. Parameters used for the visualization are $J_0 = 7200$ A/m^2, $H_0 = 0.3$ T, and $H_{max} = 0.7$ T(see text).

curve. However, the $M(H)$ for those cases can be described by the solutions obtained above. In fact, the solutions for h(r) at the field branches of $-H_p \rightarrow -H_{max}$, $-H_{max} \rightarrow -H_r$, $-H_r \rightarrow 0$, and $0 \rightarrow H_p$ are the same as in cases II, III, IV, and V, respectively, if the sign of external magnetic field changes. (We name the additional branches as cases II*, III*, IV*, and V*.)

In cylindrical coordinates, we obtain an average magnetic induction $\langle h(r) \rangle$ of a sample with radius a

$$\langle h \rangle = B = H + 4\pi M = \frac{1}{\pi a^2} \int_0^1 \int_0^{2\pi} h(r) d\theta dr .$$

As shown in Fig. 3, we visualize the field (flux) distribution inside a cylindrical superconductor with $a = 1$ mm and the corresponding profile of the critical-current density in the case of $J_0 = 7200$ A/m^2, $H_0 = 0.3$ T, and $H_{max} = 0.7$ T. The resulting $M(H)$ curve is represented in Fig. 4.

The dashed lines in Fig. 2 show our attempt to fit $M(H)$ with the exponential critical-state model. The fitting parameters, J_0 (H_0) are 31800 A/cm^2 (0.97 T), 31700 A/cm^2 (0.88 T), 30800 A/cm^2 (0.75 T), 29500 A/cm^2 (0.69 T), 20400 A/cm^2 (0.46 T), 14200 A/cm^2 (0.30 T), and 7400 A/cm^2 (0.10 T) at 5 K, 10 K, 15 K, 20 K, 25 K, 30 K, and 35 K, respectively.

The comparisons are carried out in the region where the flux jumps do not occurs. As one can see, the data are well described by the critical-state model even without considering the contribution of the reversible magneti-

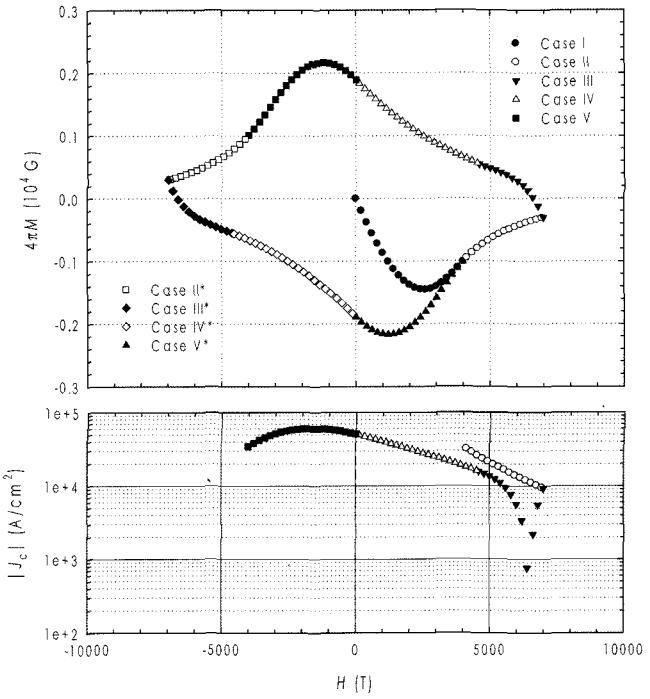

Fig. 4. Theoretical curve of magnetization $4\pi M(H)$ (top panel) and absolute value of average critical-current density $|J_c(H)|$ for $|H| \geq H_p$ (bottom panel) deduced from $h(r)$ in Fig. 3.

zation and the surface barrier effect. This implies that, in the mixed state in the MgB_2 superconductor, the magnetization mainly comes from the contribution of the bulk pinning effect.

We note that the shapes of the $M(H)$ curves shown in

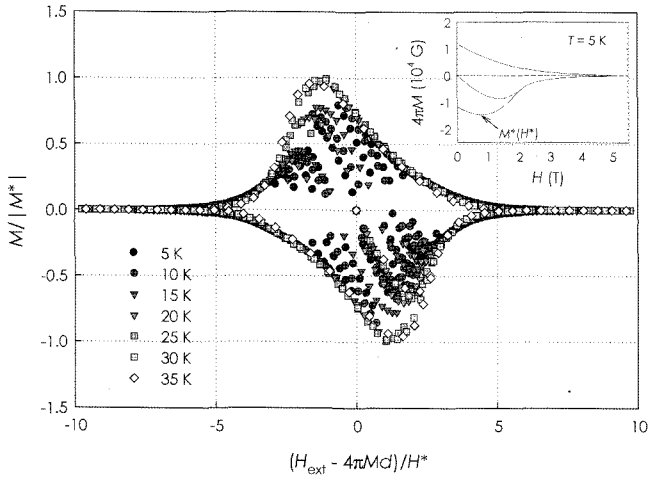

Fig. 5. Scaling of the magnetization curves, $M(T)/|M^*(T)|$ vs. H/H^*, in the temperature region 5 K $\leq T \leq$ 35 K. The inset illustrates the definitions of M^* and H^* (see text).

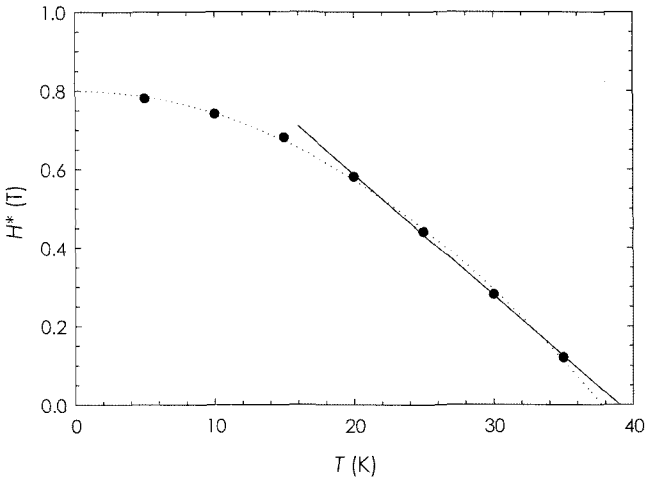

Fig. 6. Temperature dependence of phenomenological parameter H^*. Solid line represents linear least-squares fit of the data at $T \geq 20$ K, and dotted line shows $\sim 1 - (T/T_c)^2$ curve fitted to the data in 5 K $\leq$ T $\leq$ 35 K.

Fig. 2 are remarkably similar to each other, if the flux jumping regions are excluded. This suggests that the vortex pinning mechanism in MgB_2 does not change even as the temperature is varied. More concrete evidence for this can be found from the scaling analysis of the $M(H)$ curves. For the scaling of the experimental $M(H)$ curves, we get two phenomenological parameters from the theoretical $M(H)$ curves as shown in the inset of Fig. 5. $H^*(T)$ means the field where the magnetization in the increasing field branch reaches it's maximum value $M^*(T)$. We divided the M and the H in each curve of Fig. 2 by $|M^*(T)|$ and $H^*(T)$, respectively. The result is shown in Fig. 5. Except for the flux jumping regions, all the curves collapse on a single universal curve. In the case of high-T_c cuprates, such scaling behavior of the $M(H)$ curves is established in a limited low-temperature region, because the pinning mechanism determining the magnetic hysteresis changes as the temperature increases toward T_c. For $Bi_2Sr_2Ca_1Cu_2O_8$ (Bi-2212), while the bulk pinning is dominant at low temperatures, the contribution of the surface or geometrical barrier effects to the magnetization becomes more important as the temperature increases [3]. Thus, universal scaling of $M(H)$ is not seen in Bi-2212.

Figure 6 shows the temperature dependence of the scaling parameters $H^*(T)$ used in the above analysis. Since the $M(H)$ curves at various temperatures were successfully scaled with H^*, one can expect that $H^*(T)$ is proportional to the irreversibility line $H_{irr}(T)$ where the magnetic hysteresis disappears. For T $\geq$ 20 K, $H^*(T)$ is linear with respect to temperature, but the tendency deviates from the linearly as the temperature decreases. On the whole, the $H^*(T)$ shows a quadratic behavior in temperature with the downward curvature as represented by the dotted line in Fig. 6. This feature differentiates MgB_2 from the cuprates materials with $H_{irr} \sim (T_c - T)^n$ ($n \geq 1.5$) with the upward curvature.

4. Summary

In summary, we measured the magnetization curves $M(H)$ for metallic MgB_2 superconductor, which has a $T_c \simeq 39$ K, in the region 5 K $\leq T \leq$ 35 K and -5 T $\leq H \leq$ 5 T. The magnetic hysteresis in our experimental region was well described by the exponential critical-state model, without considering the reversible magnetization and the surface barrier effect. Also, we found that all the magnetization curves collapsed onto a single universal curve when the field and the magnetization were normalized by the characteristic scaling factors $H^*(T)$ and $M^*(T)$, respectively. These results lead us to the conclusion that the irreversible magnetization of MgB_2 is dominated by bulk pinning and that the pinning mechanism does not change even when the temperature is varied up to $T/T_c \simeq 0.9$.

Acknowledgements

This work was supported in part by the KRISS under Grant 05-0502-230 (Single Quantum-based Metrology in Nanoscale).

References

[1] Zhidong Hao and John R. Clem, Phys. Rev. Lett. **67**, 2371 (1991).

[2] C. P. Bean and J. D. Livingston, Rev. Mod. Phys. **36**, 31 (1964).
[3] C. D. Dewhurst, D. A. Cardwell, A. M. Campbell, R. A. Doyle, G. Balakrishnan, and D. McK. Paul, Phys. Rev. B **53**, 14594 (1996).
[4] Jun Nagamatsu, Norimasa Nakagawa, Takahiro Muranaka, Yuji Zenitani, and Jun Akimitsu, Nature **410**, 63 (2001).
[5] Kunitoshi Murai, Junya Hori, Yoshiko Fujii, Jonah Shaver, and Gregory Kozlowski, Cryogenics **45**, 415 (2005).
[6] W. A. Feitz, M. R. Beasley, J. Sicox, and W. W. Webb, Phys. Rev. **136**, A335 (1964).
[7] Y. Yeshurun, A. P. Malozemo, F. Holtzberg, and T. R. Dinger, Phys. Rev. B **38**, 11828 (1988).
[8] Min-Seok Park, C. U. Jung, J. Y. Kim, Kyung-Hee Kim, B. W. Kang, and Sung-Ik lee, Low Temp. Phys. **131**, 1165 (2003).
[9] J. A. Osborn, Phys. Rev. **67**, 351 (1945).
[10] C. H. Cheng and Y. Zhao, Physica C **386**, 31 (2003).
[11] J. H. P. Watson, J. Appl. Phys. **39**, 3406 (1968).
[12] C. P. Bean, Rev. Mod. Phys. **36**, 31 (1964).